Supporting Information

A metal–organic framework with mixed electron donor and electron acceptor ligands for efficient lithium-ion storage

Ruo-Nan Wang, Yu-Chuan Tan, Wei Liu, Zi-Yi Wang, Jun-Die Zhang, Qin-Yu Zhu*

College of Chemistry, Chemical Engineering and Materials Science, Soochow University, Suzhou 215123, P. R. China.

Corresponding Author

E-mail: zhuqinyu@suda.edu.cn;

1. Characterizations and measurements

2. Figures

Fig. S1. Crystal structures of 3D Zn-TTF/NDI MOF: (a) coordination environment of Zn2(II) ion; (b) 2D network located at ab plane constructed by the coordination of BINDI with Zn(II) ions. Hydrogen atoms are omitted for clarity.

Fig. S2. PXRD patterns of 3D Zn-TTF/NDI MOF: simulated, pristine crystals, and immersing electrolyte (ethylene carbonate (EC) and diethyl carbonate (DEC) (1:2 v/v ratio)) for 24 h.

Fig. S3. SEM images with different magnifications of crystals of 3D Zn-TTF/NDI MOF, showing the uniformity of the structures.

Fig. S4. TEM images of 3D Zn-TTF/NDI MOF, indicating the retainment of the crystallinity of the MOF after ultrasonic treatment.

Fig. S5. EDS spectra of 3D Zn-TTF/NDI MOF, indicating that the Zn/S ratio (1/2) of the crystal sample matches well with that in the formula.

Fig. S6. TGA of the crystals of 3D Zn-TTF/NDI MOF.

Fig. S7. Frontier molecular orbital distributions of 3D Zn-TTF/NDI MOF.

Fig. S8. Tauc plots for (a) direct and (b) indirect band gaps of 3D Zn-TTF/NDI MOF.

Fig. S9. Electrochemical kinetics properties of 3D Zn-TTF/NDI MOF anode: (a) CV curves vs Li/Li^+ at multiscan rates, (b) calculated *b*-values as a function of potential for lithiation and delithiation, (c) separating the capacitive current and diffusive current at a scan rate of 0.1 mV s^{-1}, (d) normalized contribution ratios of capacitive process to the total capacity at different scan rates.

Fig. S10. CV curves vs Li/Li^+ at various scan rates (a and c) and Li^+ diffusion coefficients (D_{Li}) (b and d) derived from CV curves at various scan rates for 3D Zn-TTF/NDI MOF anode (a and b) and Zn-TTF MOF anode (c and d).

Fig. S11. XPS spectra of pristine crystals of 3D Zn-TTF/NDI MOF: (a) survey scan, (b) C 1s, (c) N 1s, (d) O 1s, (e) S 2p, and (f) Zn 2p. (Black line, original data; red line, fitted data; yellow line, background).

Fig. S12. XPS spectra of 3D Zn-TTF/NDI MOF electrode after ten cycles in the fully discharged state: (a) survey scan, (b) C 1s, (c) N 1s, (d) O 1s, (e) S 2p, and (f) Zn 2p. (Black line, original data; red line, fitted data; yellow line, background).

Fig. S13. XPS spectra of 3D Zn-TTF/NDI MOF electrode after ten cycles in the fully charged state: (a) survey scan, (b) C 1s, (c) N 1s, (d) O 1s, (e) S 2p, and (f) Zn 2p. (Black line, original data; red line, fitted data; yellow line, background).

Fig. S14. SEM images of the electrodes before (a, b) and after cycling (c, d).

Fig. S15. IR spectra of pristine crystals, electrodes before and after cycling.

3. Tables

Table S1. Crystal data and structural refinement parameters for 3D Zn-TTF/NDI MOF.

Table S2. Comparison of performances of various MOFs used as LIB anodes.

1. Characterizations and measurements

1.1. General Remarks.

Compound py-TTF-py was synthesized following the previously reported method.[1] All analytically pure reagents were purchased commercially and used without further purification. Fourier transform infrared (FT-IR) spectra were recorded as KBr pellets on a Nicolet Magna 550 FT-IR spectrometer. Powder X-ray diffraction (PXRD) data of the compounds were obtained using a D/MAX-3C X-ray diffraction meter with Cu Kα (λ = 1.5406 Å) radiation. Scanning electron microscope (SEM) were recorded on SU8010 (Hitachi, Japan). Energy dispersive X-ray spectroscopy (EDS) were recorded on EVO 18 (Carl Zeiss, Germany). Thermogravimetric analysis (TGA) were performed using a TGA-DCS 6300 microanalyzer, and the sample was heated under a nitrogen stream of 100 mL min^{-1} at a heating rate of 20 °C min^{-1}. X-ray photoelectron spectroscopy (XPS) was conducted on an ESCALAB 250Xi spectrometer. Room-temperature optical diffuse reflectance spectra of the micro crystal samples were obtained with a Shimadzu UV-3150 spectrometer. The absorbance spectra were calculated from the reflectance using the Kubelka-Munk function, $\alpha/S = (1-R)^2/2R$ where R is the reflectance at a given energy, α is the absorption, and S is the scattering coefficient. Solid-state electron spin resonance (ESR) spectra were carried out at 120 K and obtained using a Bruker ER-420 spectrometer with a 100 kHz magnetic field in X band. Transmission electron microscopy (TEM) was obtained on HT7700 (Hitachi, Japan).

1.2. Preparation of Compound.

$[Zn_2(py\text{-}TTF\text{-}py)(BINDI)(DMF)_2]\bullet 3DMF\bullet EtOH\bullet 2H_2O$ (3D Zn-TTF/NDI MOF). Analytically pure reactants $Zn(NO_3)_2\cdot 6H_2O$ (0.01 mmol, 3.0 mg), py-TTF-py (0.005 mmol, 1.8 mg), and H_4BINDI (0.005 mmol, 3.0 mg) and a mixed solvent of DMF (2.7 mL) and EtOH (0.4 mL) were sealed in a thick Pyrex tube, heated at 100°C for 3 days, and then cooled to room temperature at a rate of 3 °C h^{-1}. Dark-red block crystals were obtained. The crystals were rinsed with DMSO and DMF and hand-picked under a microscope. The yield of the crystals is 32.7 % (2.5 mg) based on

H_4BINDI. IR data (cm^{-1}): 1709(m), 1675(w), 1655(s), 1611(s), 15776(m), 1552(m), 1534(w), 1495(w), 1432(m), 1404(w), 1384(m), 1341(vs), 1244(s), 1206(w), 1185(m), 1099(m), 1070(m), 1028(m), 982(w), 938(w), 879(w), 822(m), 775(m), 766(m), 741(m), 726(m), 691(m), 652(s), 630(m).

1.3. X-ray Crystallographic Study.

The crystal data were collected using a Bruker APEX-II CCD diffractometer equipped with graphite monochromated Mo Kα (λ = 0.71075 Å) radiation were used to carry out the measurements. The structures were solved by direct methods using SHELXS-18 program and the refinements were performed against F^2 using SHELXL-16. All the nonhydrogen atoms are refined anisotropically. The hydrogen atoms are positioned with idealized geometry and refined with fixed isotropic displacement parameters.

1.4. Theoretical Calculations

Density functional theory calculations were carried out using GAUSSIAN 16 program package for 3D Zn-TTF/NDI MOF at the B3LYP level. The basis set used for C, N, O, S and H atoms was 6-311G*. Considering that in the –D–A– packing column, the D would interact with the adjacent A above and below, and the same case for A, therefore, the input packing D–A–D–A column extracted from the single crystal structure of 3D Zn-TTF/NDI MOF was used as the initial model.

1.5. Electrochemical Characterization.

To prepare MOF electrodes, 3D Zn-TTF/NDI MOF crystals were ground into powders that were mixed with Super P and poly(vinylidene fluoride) (PVDF) binder in N-methyl-2-pyrrolidone (NMP) with a mass ratio of 6:3:1, respectively. After stirring for over 10 h, homogenous slurry was coated on a Cu foil, dried at 60 ℃ overnight, cut into circular disks (13 mm in diameter for half-cell), and then dried under vacuum at 120 ℃ overnight. The electrodes were stored in an Ar-filled glove box where the moisture and oxygen concentrations were strictly limited to below 0.1 ppm. 1.0 mol L^{-1} $LiPF_6$ in ethylene carbonate (EC) and diethyl carbonate (DEC) (1:2

v/v ratio) as the electrolyte, and Celgard 2500 as the separator were used to assemble a CR2032 coin cell. For the assembly of half-cells, Li foils were used as the counter electrode. The area mass loading of the active material in half-cells was in the range of 0.3–0.5 mg cm^{-2}.

CV measurements were conducted on a Chenhua CHI760E electrochemical workstation. The half-cells were tested within the voltage range of 0.01–3.0 V. EIS measurements were carried out on a ZAHNER ENNIUM workstation in the frequency range from 100 kHz to 0.01 Hz with the amplitude of 5 mV. The cycling and rate performances of the cells were measured on a LAND CT2001A analyzer at different current densities. The specific capacities were calculated according to the loading mass of active materials.

References

(1) Han, Y.-F.; Zhang, J.-S.; Lin, Y.-J.; Dai, J.; Jin, G.-X. Synthesis and Characterization of Half-Sandwich Iridium Complexes Containing 2,6(7)-bis(4-pyridyl)-1,4,5,8-Tetrathiafulvalene and Ancillary Ortho-Carborane-1,2-Dichalcogenolato Ligands. *J. Organomet. Chem.* **2007**, *692*, 4545–4550.

2. Figures:

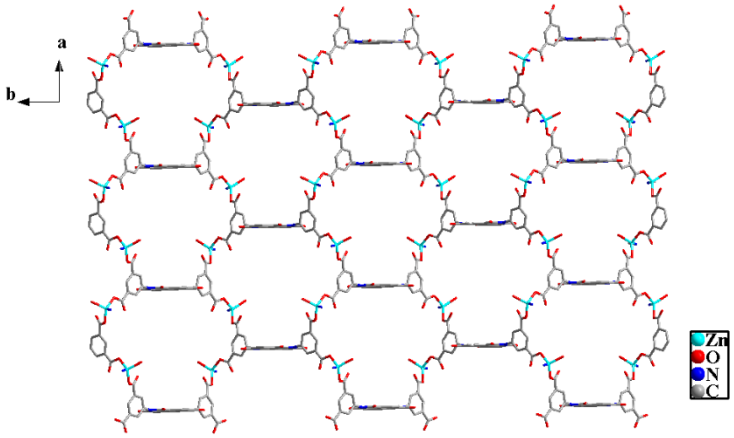

Fig. S1. 2D network located at ab plane constructed by the coordination of BINDI with Zn(II) ions. Hydrogen atoms are omitted for clarity.

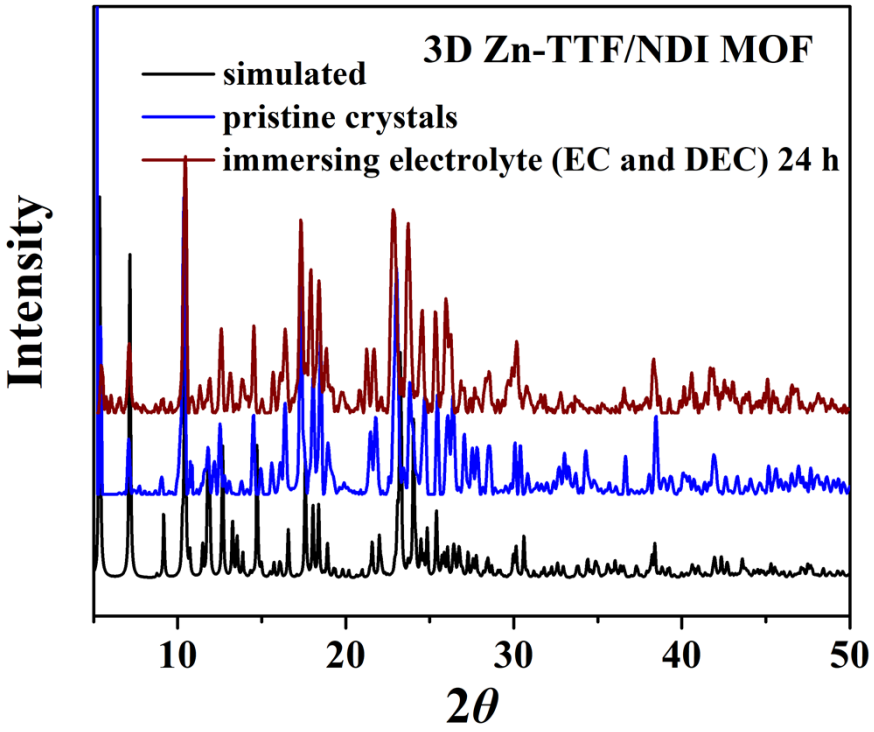

Fig. S2. PXRD patterns of 3D Zn-TTF/NDI MOF: simulated, pristine crystals, and immersing electrolyte (ethylene carbonate (EC) and diethyl carbonate (DEC) (1:2 v/v ratio)) for 24 h.

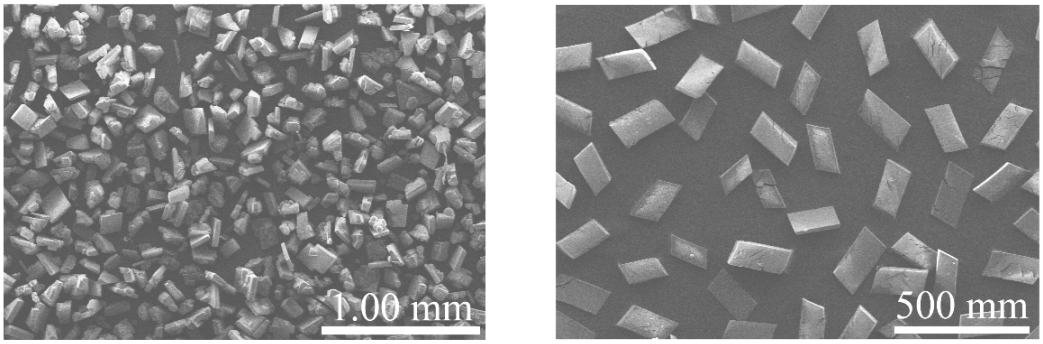

Fig. S3. SEM images with different magnifications of crystals of 3D Zn-TTF/NDI MOF, showing the uniformity of the structures.

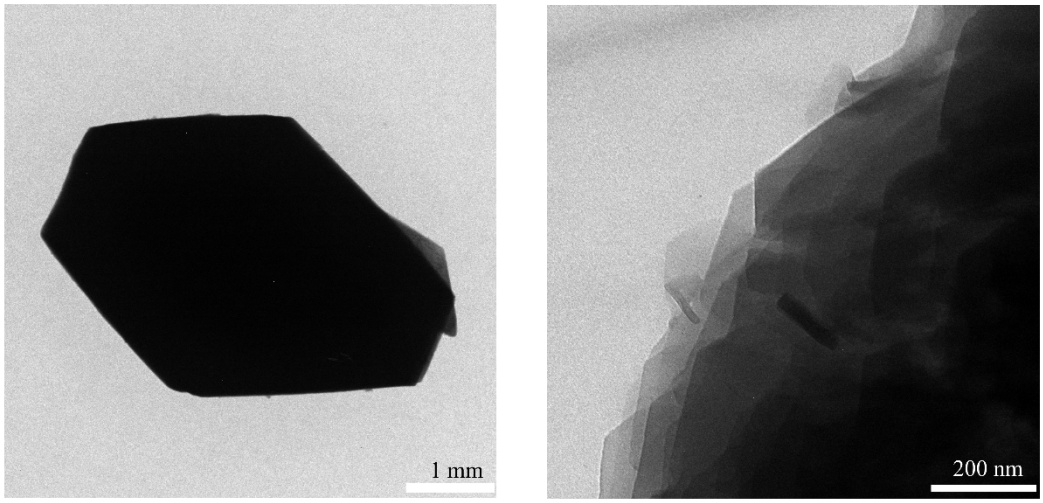

Fig. S4. TEM images of 3D Zn-TTF/NDI MOF, indicating the retainment of the crystallinity of the MOF after ultrasonic treatment.

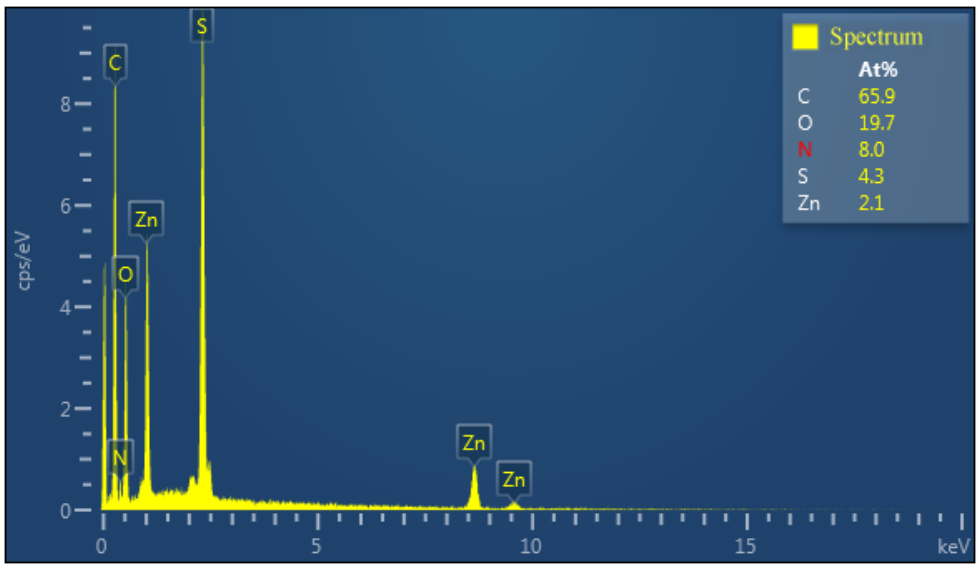

Fig. S5. EDS spectra of 3D Zn-TTF/NDI MOF, indicating that the Zn/S ratio (1/2) of the crystal sample matches well with that in the formula.

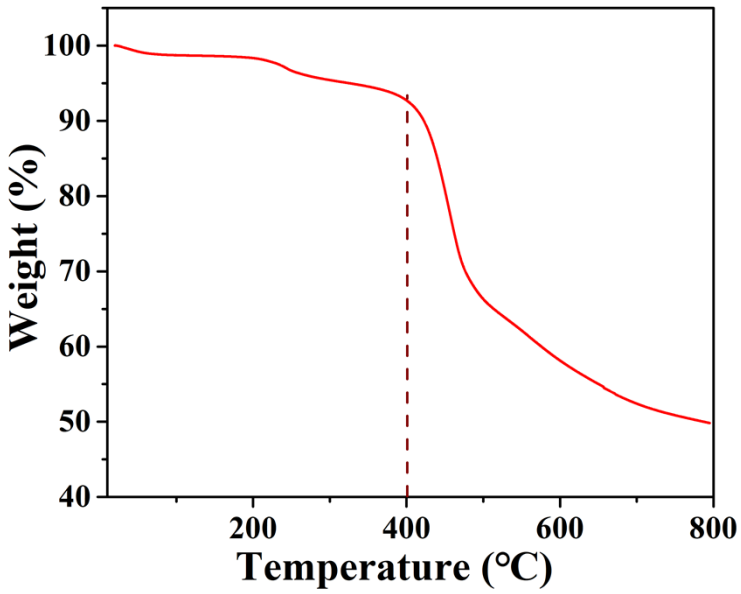

Fig. S6. TGA of the crystals of 3D Zn-TTF/NDI MOF.

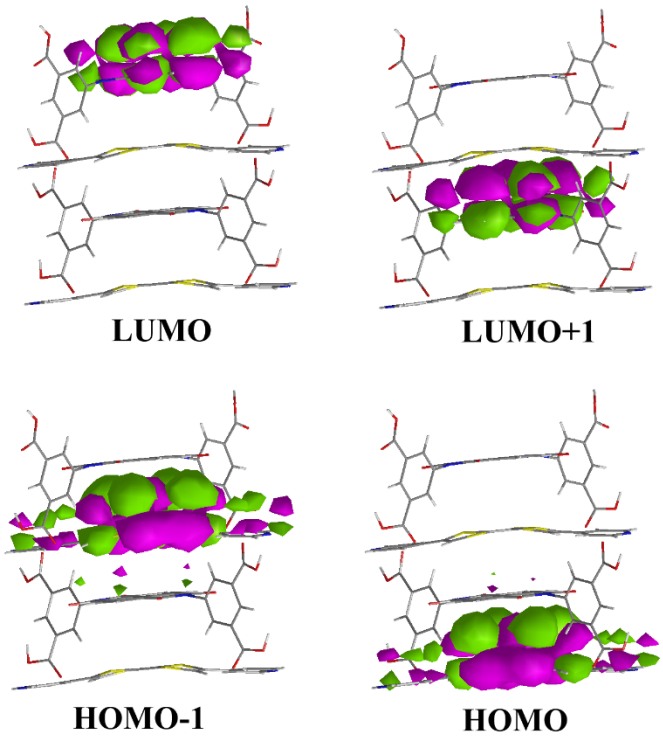

Fig. S7. Frontier molecular orbital distributions of 3D Zn-TTF/NDI MOF.

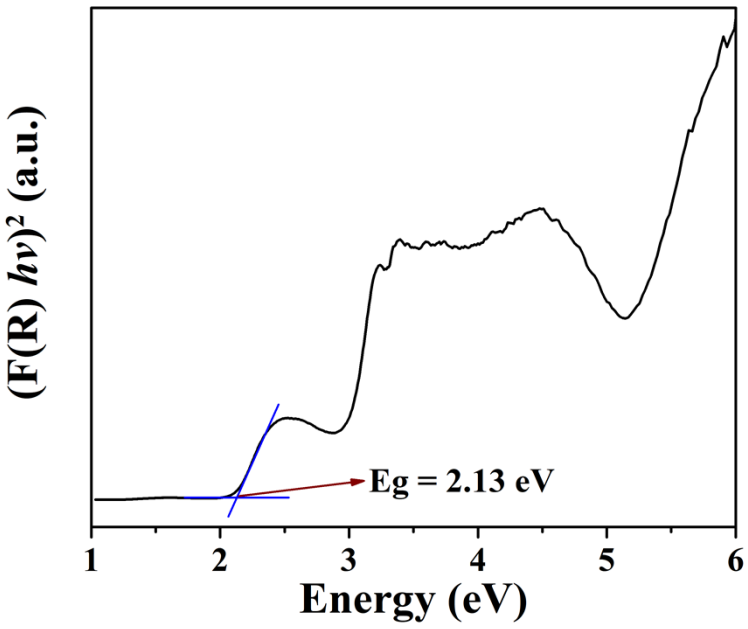

(a)

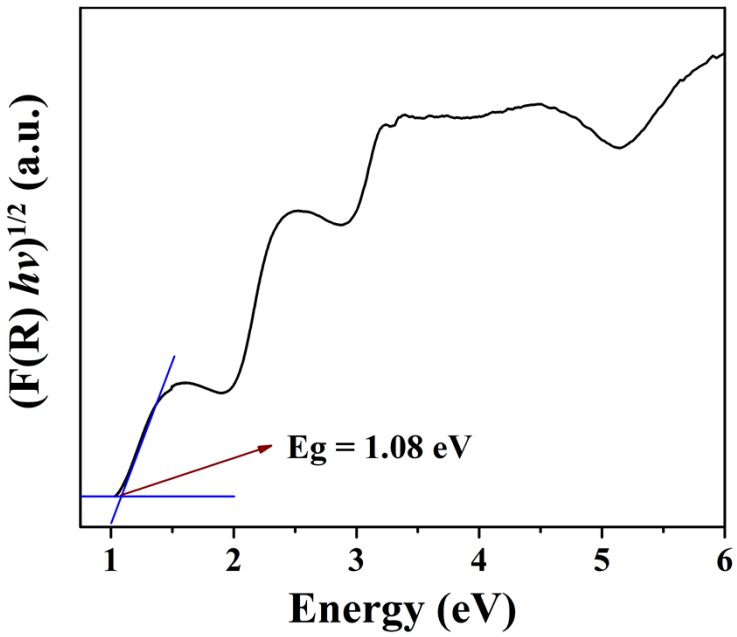

(b)

Fig. S8. Tauc plots for (a) direct and (b) indirect band gaps of 3D Zn-TTF/NDI MOF.[1]

1. Sippel, P.; Denysenko, D.; Loidl, A.; Lunkenheimer, P.; Sastre, G.; Volkmer, D. Dilectric Relaxation Processes, Electronic Structure, and Band Gap Engineering of MFU-4-type Metal−Organic Frameworks: Towards a Rational Design of Semiconducting Microporous Materials. *Adv. Funct. Mater.* **2014**, *24*, 3885−3896.

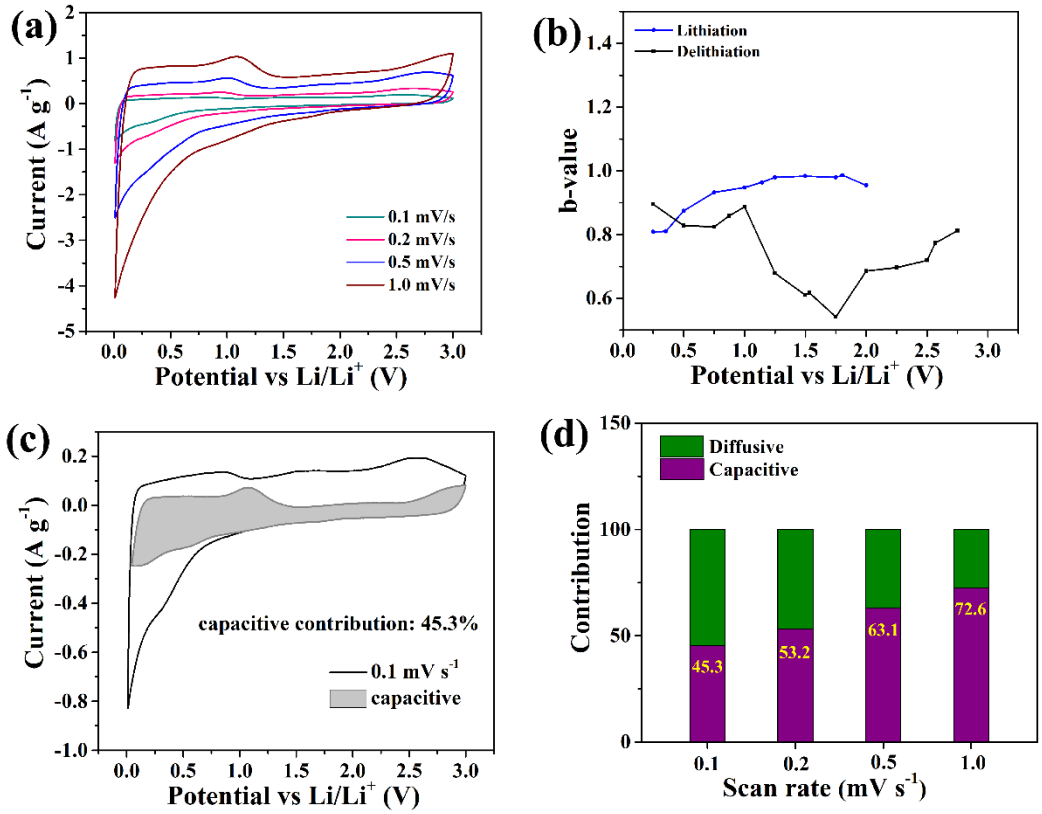

Fig. S9. Electrochemical kinetics properties of 3D Zn-TTF/NDI MOF anode: (a) CV curves vs Li/Li^+ at multiscan rates, (b) calculated *b*-values as a function of potential for lithiation and delithiation, (c) separating the capacitive current and diffusive current at a scan rate of 0.1 mV s^{-1}, (d) normalized contribution ratios of capacitive process to the total capacity at different scan rates.

To explore the electrochemical reaction kinetics and to evaluate the quantitative contributions of diffusive and capacitive behaviors of 3D Zn-TTF/NDI MOF anode, CV at multi-scan rates from 0.1 to 1.0 mV s^{-1} was performed and shown in Fig. S6a. The relationship between peak current (i) and scan rate (v) is described by the power law:[1–3]

$$i = av^b \qquad (1)$$

The b values could be calculated from the slope of the fitted line of log(i) versus log(v). The b values of 0.5 and 1.0 indicate a totally diffusion controlled behavior (battery-type) and an ideally capacitive controlled mechanism, respectively. As for the 3D Zn-TTF/NDI MOF anode case, the b values as a function of potential for lithiation/delithiation process are shown in Fig. S6b. Most b values are in the range of 0.6–0.9, indicating that both the capacitive and diffusive behaviors are involved in the charge–discharge processes. The surface-capacitive and diffusive contributions at various scan rates (Fig. S6c and d) are evaluated using k_1v and $k_2v^{1/2}$ in the equation:[4,5]

$$i = k_1v + k_2v^{1/2}$$

As demonstrated in Fig. S6d, the calculated capacitive contribution at 0.5 mV s^{-1} is approximately 63.1%, which occupies a high fraction of the total capacity. It can be seen that the percentage of capacitive contribution of the 3D Zn-TTF/NDI MOF anode increases with increasing scan rates from 0.1 to 1.0 mV s^{-1}, finally reaches 72.6% at 1.0 mV s^{-1}. This remarkable feature is highly beneficial for rapid lithium ion storage, leading to the excellent storage properties, especially at high rates.

References:

1. K. M. Hercule, Q. L. Wei, O. K. Asare, L. B. Qu, A. M. Khan, M. Y. Yan, C. H. Du, W. Chen and L. Q. Mai, *Adv. Energy Mater.*, 2015, **5**, 1500060.
2. C. T. Zhao, C. Yu, M. D. Zhang, H. W. Huang, S. F. Li, X. T. Han, Z. B. Liu, J. Yang, W. Xiao, J. N. Liang, X. L. Sun and J. S. Qiu, *Adv. Energy Mater.*, 2017, **7**, 1602880.
3. H. W. Wang, Y. Zhang, H. X. Ang, Y. Q. Zhang, H. T. Tan, Y. F. Zhang, Y. Y. Guo, J. B. Franklin, X. L. Wu, M. Srinivasan, H. J. Fan and Q. Y. Yan, *Adv. Funct. Mater.*, 2016, **26**, 3082–3093.
4. Q. B. Guo, Y. F. Ma, T. T. Chen, Q. Y. Xia, M. Yang, H. Xia and Y. Yu, *ACS Nano*, 2017, **11**, 12658–12667.
5. Y. Liu, Y. J. Fang, Z. W. Zhao, C. Z. Yuan and X. W. Lou, *Adv. Energy Mater.*, 2019, **9**, 1803052.

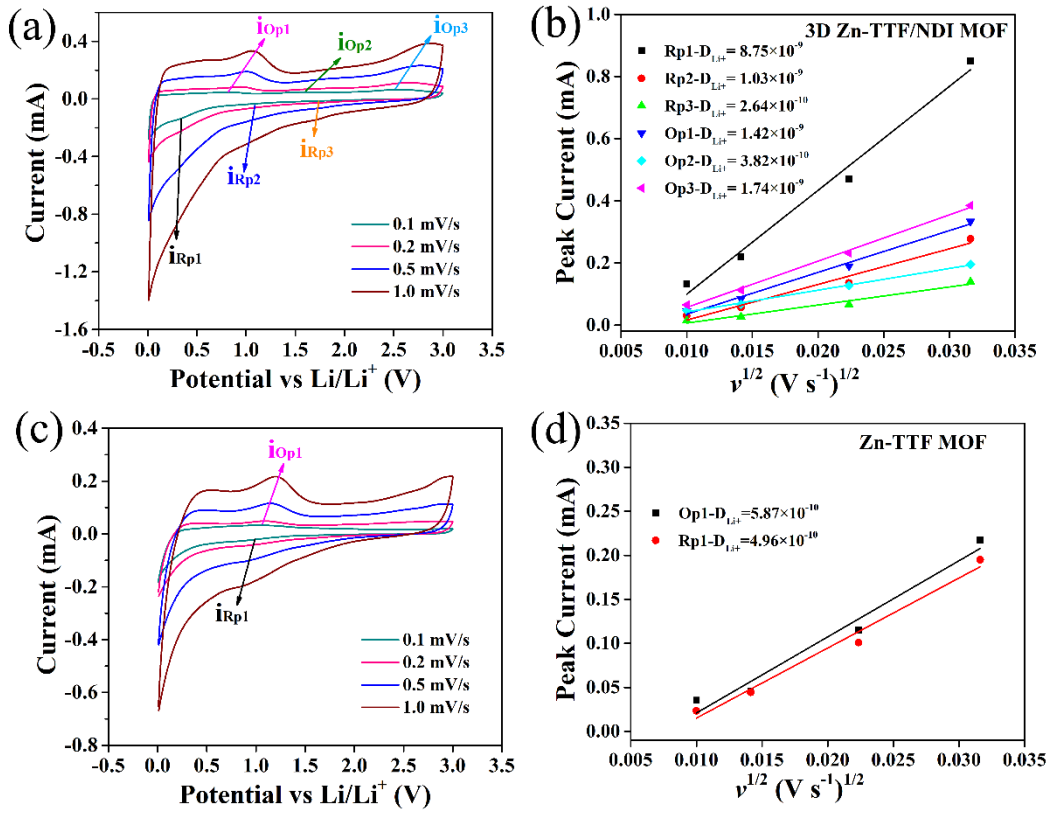

Fig. S10. CV curves vs Li/Li^+ at various scan rates (a and c) and Li^+ diffusion coefficients (D_{Li}) (b and d) derived from CV curves at various scan rates for 3D Zn-TTF/NDI MOF anode (a and b) and Zn-TTF MOF anode (c and d).

Li ion diffusion coefficient (D_{Li}) calculation:

D_{Li} was calculated following the Randles-Sevcik equation: [1,2]

$$i_P = (2.69 \times 10^5) n^{\frac{3}{2}} A D_{Li}^{\frac{1}{2}} C_{Li} v^{\frac{1}{2}}$$

where i_P is the peak current, n is the charge-transfer number, A is the area of electrode/electrolyte interface, C_{Li} is the concentration of Li^+ in the electrode, and v is the potential scan rate.

References:

1. Jin, H.; Xin, S.; Chuang, C.; Li, W.; Wang, H.; Zhu, J.; Xie, H.; Zhang, T.; Wan, Y.; Qi, Z.; Yan, W.; Lu, Y.-R.; Chan, T.-S.; Wu, X.; Goodenough, J. B.; Ji, H.; Duan, X. Black Phosphorus Composites with Engineered Interfaces for High-Rate High-Capacity Lithium Storage. *Science* **2020**, *370*, 192–197.

2. A. J. Bard, L. R. Faulkner, *Electrochemical Methods: Fundamentals and Applications* (2nd ed., Wiley, **2001**), chap. 6.

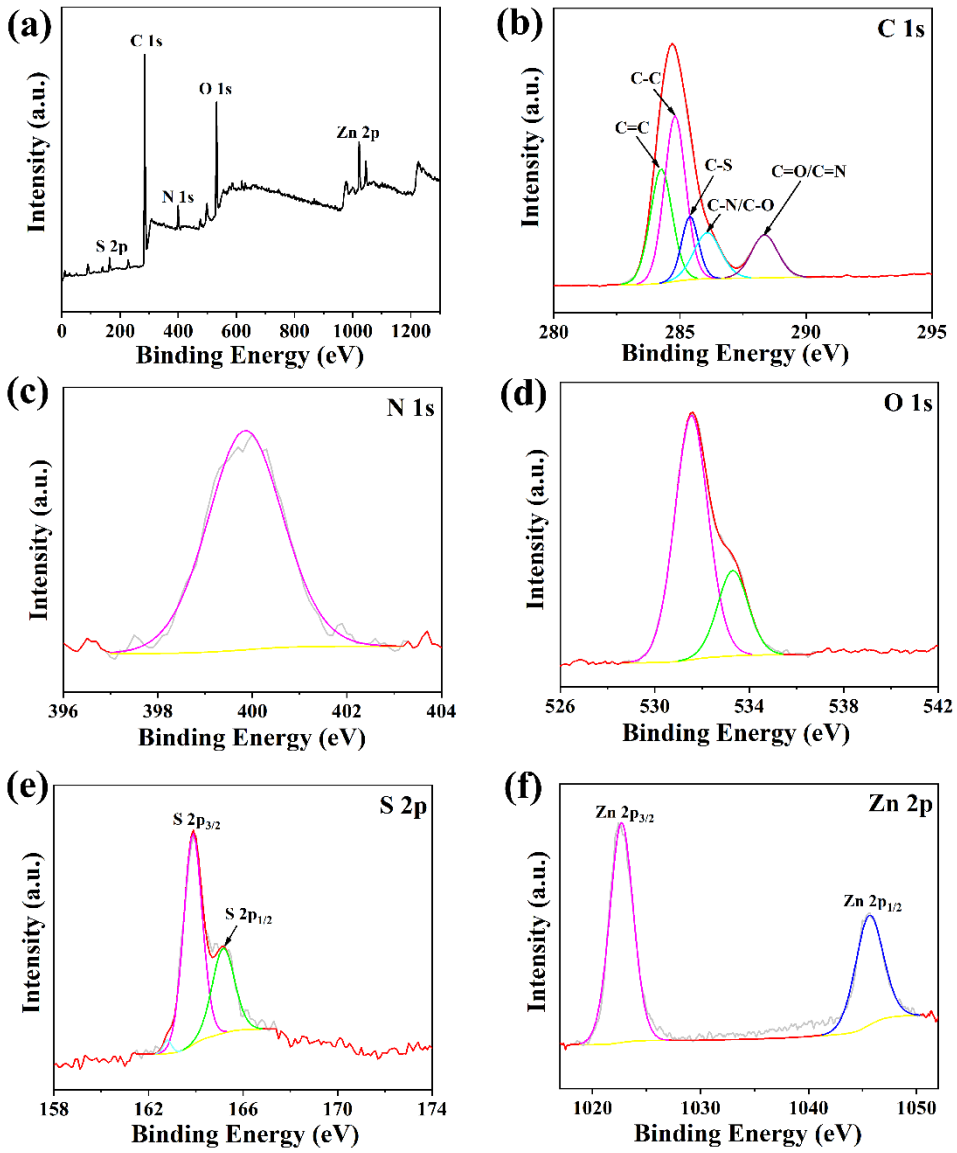

Fig. S11. XPS spectra of pristine crystals of 3D Zn-TTF/NDI MOF: (a) survey scan, (b) C 1s, (c) N 1s, (d) O 1s, (e) S 2p, and (f) Zn 2p. (Black line, original data; red line, fitted data; yellow line, background).

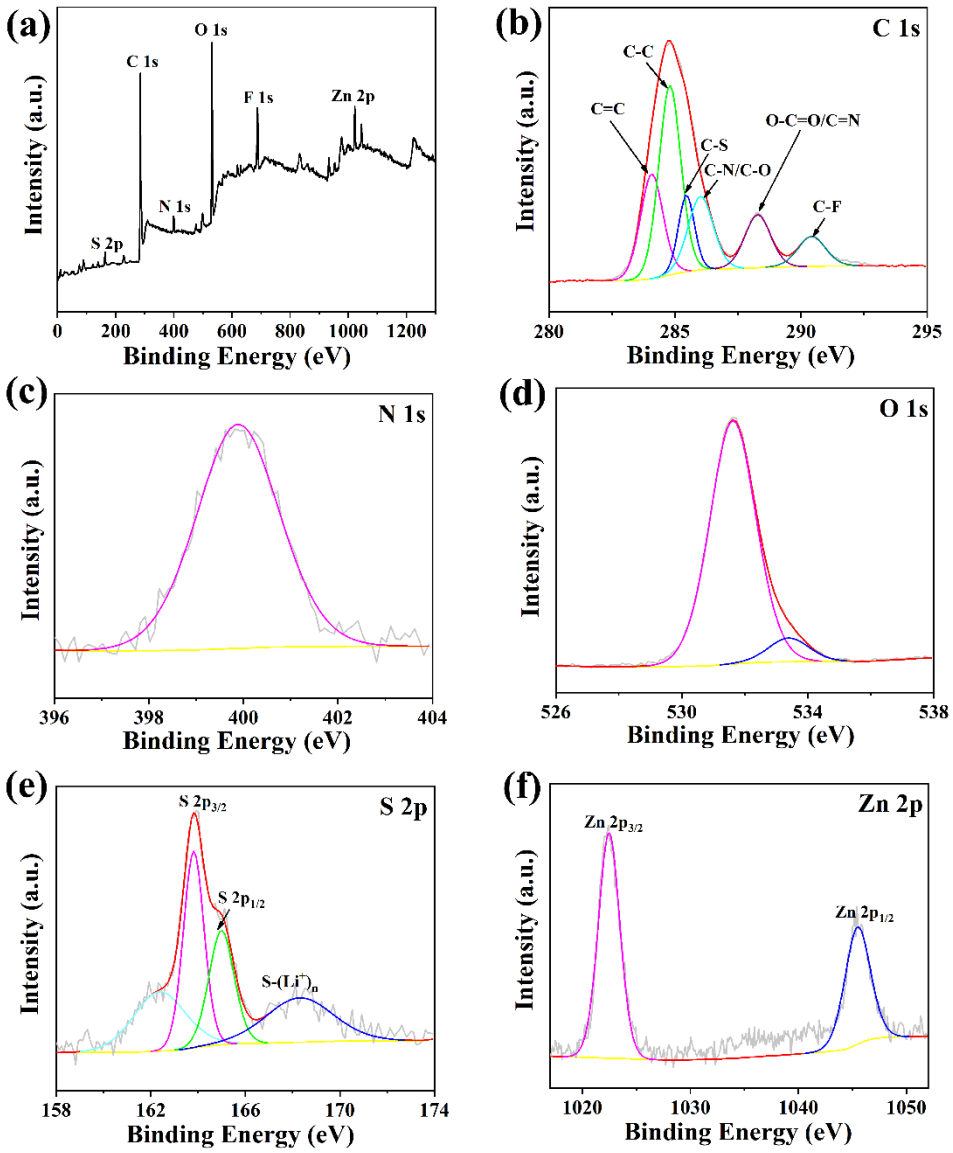

Fig. S12. XPS spectra of 3D Zn-TTF/NDI MOF electrode after ten cycles in the fully discharged state: (a) survey scan, (b) C 1s, (c) N 1s, (d) O 1s, (e) S 2p, and (f) Zn 2p. (Black line, original data; red line, fitted data; yellow line, background).

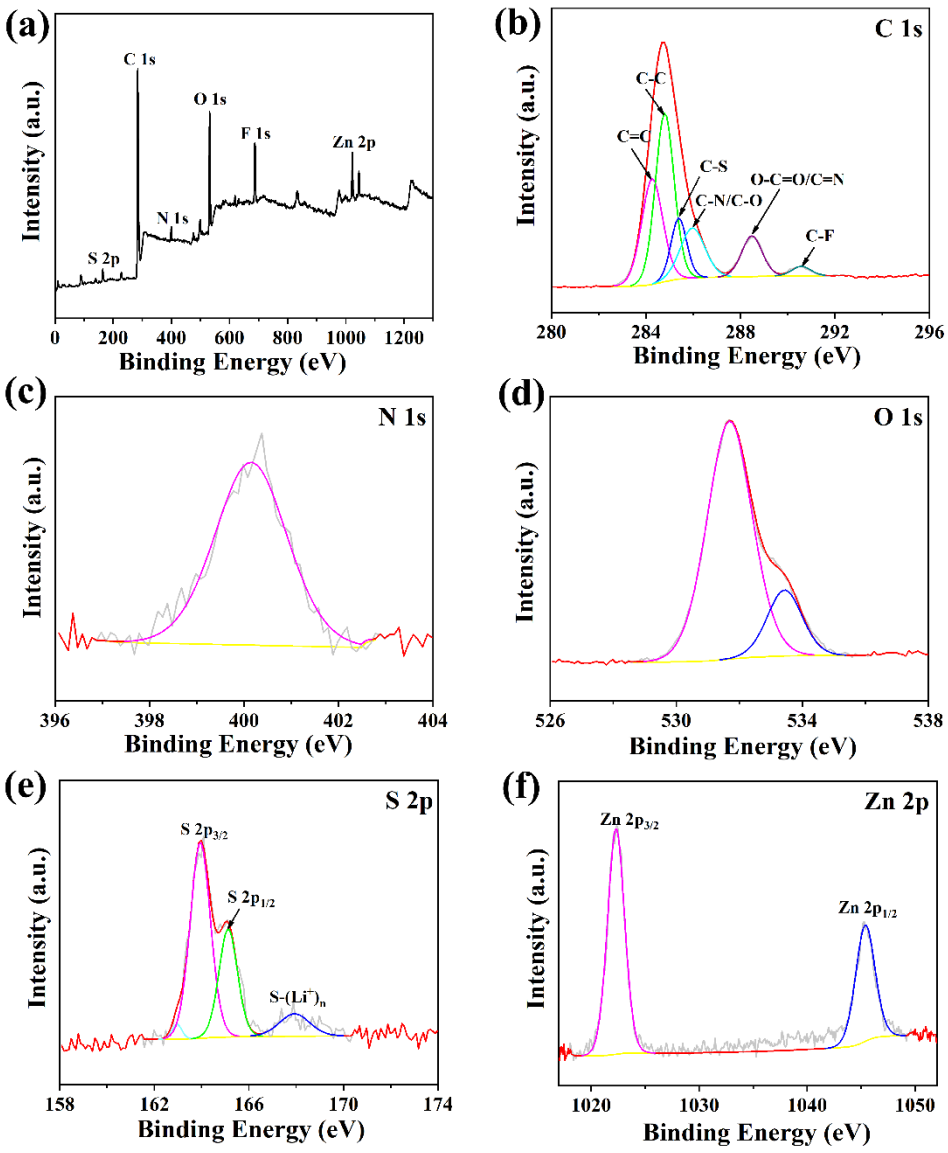

Fig. S13. XPS spectra of 3D Zn-TTF/NDI MOF electrode after ten cycles in the fully charged state: (a) survey scan, (b) C 1s, (c) N 1s, (d) O 1s, (e) S 2p, and (f) Zn 2p. (Black line, original data; red line, fitted data; yellow line, background).

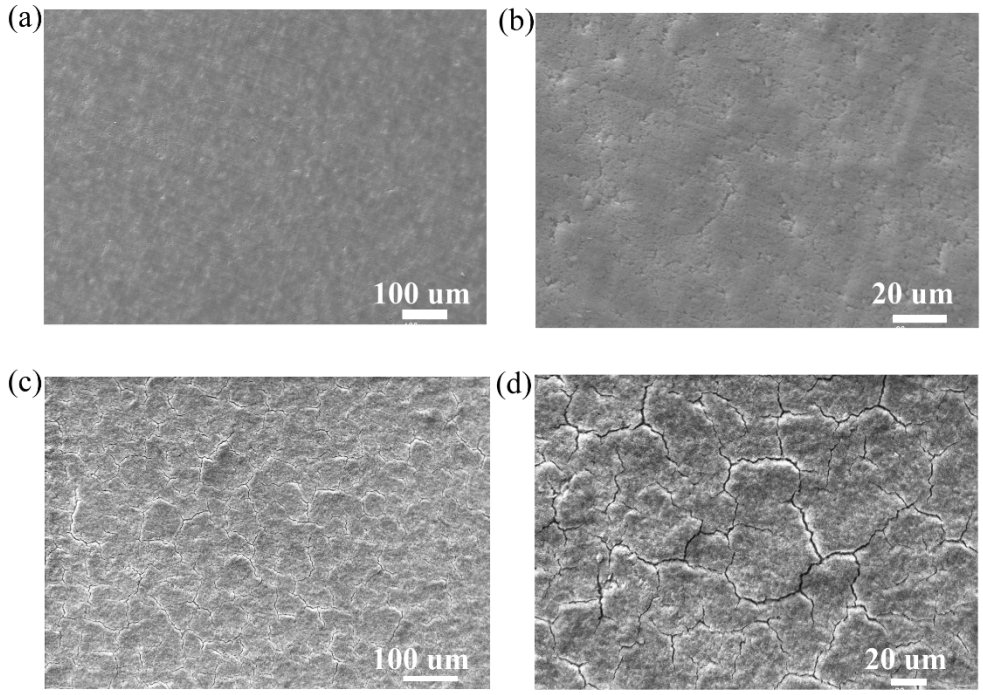

Fig. S14. SEM images of the electrodes before (a, b) and after cycling (c, d).

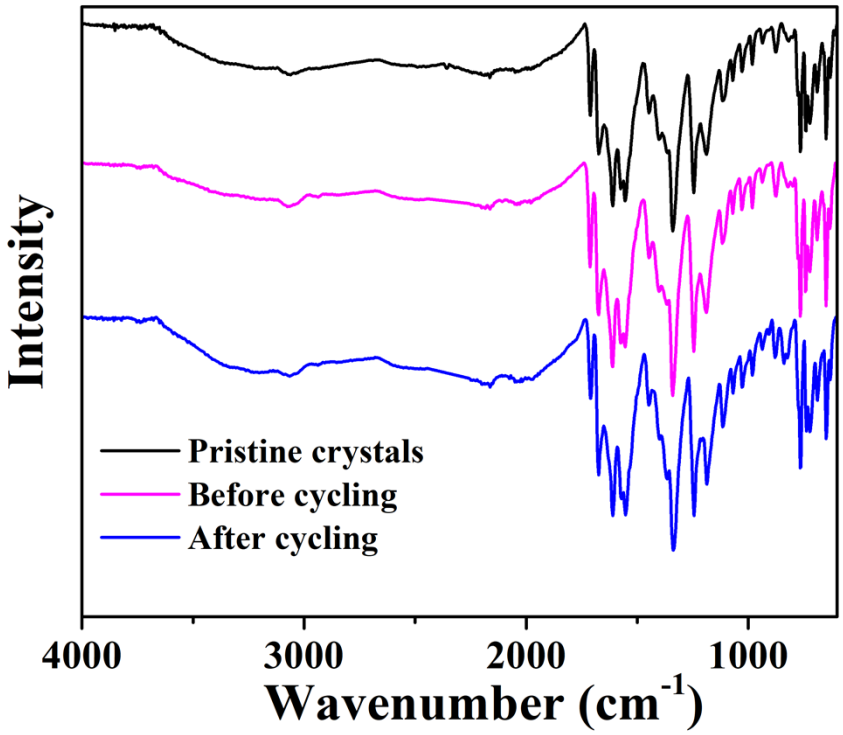

Fig. S15. IR spectra of pristine crystals, electrodes before and after cycling.

3. Tables

Table S1. Crystal data and structural refinement parameters for 3D Zn-TTF/NDI MOF.

	3D Zn-TTF/NDI MOF
formula	$C_{29}H_{26}N_4O_8S_2Zn$
fw	688.031
cryst size (mm^3)	0.04×0.12×0.22
cryst syst	orthorhombic
space group	*Pccn*
a (Å)	32.9631(15)
b (Å)	13.3189(6)
c (Å)	15.4095(7)
α (deg)	90
β (deg)	90
γ (deg)	90
V ($Å^3$)	6765.3(5)
Z	8
ρ_{calcd} ($g\ cm^{-3}$)	1.347
F(000)	2816
μ (mm^{-1})	0.904
T (K)	100(2)
reflns collected	157739
unique reflns	5911
observed reflns	5330
no. params	406
GOF on F^2	1.176
R_1 [I>2σ(*I*)]	0.1277
${}_wR_2$ [I>2σ(*I*)]	0.2662

Table S2. Comparison of performances of various MOFs used as LIB anodes.

	MOFs	Capacity (mA h g^{-1})	Current density (mA g^{-1})	Cycle number	Capacity @ Max Current Rate (mA g^{-1})	Reference
1	$Zn(IM)_{1.5}(abIM)_{0.5}$	190	100	200	75@400	[1]
2	Mn-BTC MOF	694	103	100	400@1000	[2]
3	Ni-Me_4bpz	120	50	100		[3]
4	Co-BTC-EtOH MOF	473	2000	500		[4]
5	Co-MOF	1021	100	200	435@1000	[5]
6	UiO 66	190	38.8	30	50@980	[6]
7	Fe-MIL-88B	744	60	400	133@5000	[7]
8	Pb-MOF	489	100	500		[8]
9	Mn-MOF	600	100	200	300@1000	[9]
10	Ni-BHC	1261.3	100	50		[10]
11	MOF-74 (Fe, Co, Ni)	456	1000	500	440@2000	[11]
12	Fe-MOF	728	50	1100	500@3000	[12]
13	Ni-MOF	765	100	140	313@2000	[13]
14	Mn-MOF	255	100	200		[14]
15	Co-MOF	732	100	200	45@2000	[14]
16	Zn-MOF	112	100	200		[14]
17	$[Co(TTPA)_3(TDC)_2(H_2O)]$ ·4DMF·$3H_2O$	210	500	1000	55@2000	[15]
18	$[Ni(TTPA)_3(TDC)_2(H_2O)]$ ·3DMF·H_2O	146	500	1000	50@2000	[15]
19	Ni−Mn−BPTC-e-MOFs	1269	100	200	736@6000	[16]
20	Ni-Mn-BPTC-g-MOFs	421	100	200	185@6000	[16]
21	$Co(BDC)TED_{0.5}$@24h	808.2	1000	1000		[17]
22	Ni-MOF NF	733	1000	200	84@50000	[18]
23	TTF-Zn-MOF **1**	1117.4	200	150	722.1@20000	[19]
24	TTF-Zn-MOF **2**	621.3	200	70	314.3@20000	[19]
25	TTF-Co-MOF **1**	1186.6	200	287	655.7@20000	[20]
26	TTF-Co-MOF **2**	1070.9	200	174		[20]
27	TTFTB-MnCo- MOF	1123.9	200	191	928.7@20000	[21]
28	TTFTB-Mn- MOF	883.2	200	182		[21]
29	TTFTB-Co- MOF	962.6	200	160		[21]
30	Zr–MOF **1**	561	100		108@2000	[22]
31	Zr–MOF **2**	434	100		60@2000	[22]
32	Zr–MOF **3**	374	100		62@2000	[22]
33	Mn–o–TTFOB	1249	200	after full activation	836@2000	[23]
34	Zn–o–TTFOB	1288	200	after full activation	813@2000	[23]

35	Cd–o–TTFOB	448	200	after full activation	262@2000	[23]
	3D Zn-TTF/NDI MOF	1402	200	400	844.4@20000	This work
		956	1000	600		
		625	5000	900		

References

1. Y. Lin, Q. Zhang, C. Zhao, H. Li, C. Kong, C. Shen and L. Chen, *Chem. Commun.*, 2015, **51**, 697–699.

2. S. Maiti, A. Pramanik, U. Manju and S. Mahanty, *ACS Appl. Mater. Interfaces*, 2015, **7**, 16357–16363.

3. T. C. An, Y. H. Wang, J. Tang, Y. Wang, L. J. Zhang and G. F. Zheng, *J. Colloid Interface Sci.*, 2015, **445**, 320–325.

4. C. Li, X. Lou, M. Shen, X. Hu, Z. Guo, Y. Wang, B. Hu and Q. Chen, *ACS Appl. Mater. Interfaces*, 2016, **8**, 15352–15360.

5. C. Li,; X. Hu, X. Lou, L. Zhang, Y. Wang, J.-P. Amoureux, M. Shen, Q. Chen and B. Hu, J. *Mater. Chem. A*, 2016, **4**, 16245–16251.

6. B. Tang, S. Huang, Y. Fang, J. Hu, C. Malonzo, D. G. Truhlar and A. Stein, *J. Chem. Phys.*, **2016**, **144**, 194702.

7. L. Shen, H. Song and C. Wang, *Electrochim. Acta*, 2017, **235**, 595–603.

8. L. Hu, X.-M. Lin, J.-T. Mo, J. Lin, H.-L. Gan, X.-L. Yang and Y.-P. Cai, *Inorg. Chem.*, 2017, **56**, 4289–4295.

9. T. Gong, X. Lou, E. Q. Gao and B. Hu, *ACS Appl. Mater. Interfaces.*, 2017, **9**, 21839–21847.

10. X. Lou,; Y. Ning, C. Li, M. Shen, B. Hu, X. Hu and B. Hu, *Inorg. Chem.*, 2018, **57**, 3126–3132.

11. D. Zhou, J. Ni and L. Li, *Nano Energy*, 2019, **57**, 711–717.

12. Sharma, N. S. Szunerits, R. Boukherroub, R. Ye, S. Melinte, M. O. Thotiyl and S. Ogale, *ACS Appl. Energy Mater.*, 2019, **2**, 4450−4457.

13. L. Zhang, X. Zhang,; D. Han and S. Wu, *Inorg. Chem. Commun.*, 2023, **158**, 111511.

14. N. Sharmawipawekul, N. Kaeosamut, T. Autthawong, A. Watwiangkham, S. Suthirakun, S. Wannapaiboon, N. Mahamai, T. Sarakonsri, Y. Chimupala and S. Yimklan, *Chem. Eng. J.*, 2024, **482**, 148904.

15. C. M. Ngue, F. Baskoro, H. Q. Wong, H. J. Yen and M. K. Leung, *Cryst. Growth Des.*, 2022, **22**, 5872–5882.

16. C.-J. Yin, L.-F. Xu, Y.-S. Pan and C.-L. Pan, *ACS Appl. Energy Mater.*, 2020, **3**, 10776–10786.

17. S. Mutahir, C. X. Wang, J. J. Song, L. Wang, W. Lei, X. Y. Jiao, M. A. Khan, B. J. Zhou, Q. Zhong and Q. L. Hao, *Appl. Mater. Today*, 2020, **21**, 100813.

18. A. Nazir, H. T.T. Le, A.-G. Nguyen and C.-J. Park, *Electrochim. Acta*, 2021, **389,** 138750.

19. Y.-G. Weng, W.-Y. Yin, M. Jiang, J.-L. Hou, J. Shao, Q.-Y. Zhu and J. Dai, *ACS Appl. Mater. Interfaces*, 2020, **12**, 52615−52623.

20. Y.-G. Weng, Z.-H. Ren, Z.-R. Zhang, J. Shao, Q.-Y. Zhu and J. Dai, *Inorg. Chem.*, 2021, **60**, 17074−17082.

21. L.-J. Ma, C.-Y. Luo, R.-N. Wang, Y.-C. Tan, J.-L. Hou and Q.-Y. Zhu, *ACS Energy Lett.*, 2023, **8**, 4427–4437.

22. W. Yan, J. Su, Z.-M. Yang, S. Lv, Z. Jin and J.-L. Zuo, *Small*, 2021, **17**, 2005209.

23. Z.-M. Yang, S.-P. Zhao, M.-H. Zhang, Z.-D. Zhang, T.-R. Ma, S. Yuan, J. Su,; C.-H. Li and J.-L. Zuo, *Angew. Chem. Int. Ed.*, 2023, **62**, e202304183.